Am J Nucl Med Mol Imaging 2014;4(3):231-238
www.ajnmmi.us /ISSN:2160-8407/ajnmmi1401001

*Original Article*

# Relationship between pretreatment FDG-PET and diffusion-weighted MRI biomarkers in diffuse large B-cell lymphoma

Antoinette de Jong[1], Thomas C Kwee[1], John MH de Klerk[2], Judit A Adam[3,9], Bart de Keizer[1], Rob Fijnheer[4], Marie José Kersten[5], Inge Ludwig[6], Yvonne WS Jauw[7], Josée M Zijlstra[7], Indra C Pieters - Van den Bos[8], Jaap Stoker[9], Otto S Hoekstra[10], Rutger AJ Nievelstein[1]

*[1]Department of Radiology and Nuclear Medicine, University Medical Center, Utrecht, The Netherlands; [2]Department of Nuclear Medicine, Meander Medical Center, Amersfoort, The Netherlands; [3]Department of Nuclear Medicine, Academic Medical Center, Amsterdam, The Netherlands; [4]Department of Hematology, Meander Medical Center, Amersfoort, The Netherlands; [5]Department of Hematology, Academic Medical Center, Amsterdam, The Netherlands; [6]Department of Hematology, University Medical Center Utrecht, Utrecht, The Netherlands; [7]Department of Hematology, VU University Medical Center, Amsterdam, The Netherlands; [8]Department of Radiology, VU University Medical Center, Amsterdam, The Netherlands; [9]Department of Radiology, Academic Medical Center, Amsterdam, The Netherlands; [10]Department of Radiology and Nuclear Medicine, VU University Medical Center Amsterdam, The Netherlands*

Received January 5, 2014; Accepted February 11, 2014; Epub April 25, 2014; Published April 30, 2014

**Abstract:** The purpose of this study was to determine the correlation between the $^{18}$F-fluoro-2-deoxy-D-glucose positron emission tomography (FDG-PET) standardized uptake value (SUV) and the diffusion-weighted magnetic resonance imaging (MRI) apparent diffusion coefficient (ADC) in newly diagnosed diffuse large B-cell lymphoma (DLBCL). Pretreatment FDG-PET and diffusion-weighted MRI of 21 patients with histologically proven DLBCL were prospectively analyzed. In each patient, maximum, mean and peak standardized uptake value (SUV) was measured in the lesion with visually highest FDG uptake and in the largest lesion. Mean ADC ($ADC_{mean}$, calculated with b-values of 0 and 1000 s/mm$^2$) was measured in the same lesions. Correlations between FDG-PET metrics ($SUV_{max}$, $SUV_{mean}$, $SUV_{peak}$) and $ADC_{mean}$ were assessed using Pearson's correlation coefficients. In the lesions with visually highest FDG uptake, no significant correlations were found between the $SUV_{max}$, $SUV_{mean}$, $SUV_{peak}$ and the $ADC_{mean}$ ($P$=0.498, $P$=0.609 and $P$=0.595, respectively). In the largest lesions, there were no significant correlations either between the $SUV_{max}$, $SUV_{mean}$, $SUV_{peak}$ and the $ADC_{mean}$ ($P$=0.992, $P$=0.843 and $P$=0.894, respectively). The results of this study indicate that the glycolytic rate as measured by FDG-PET and changes in water compartmentalization and water diffusion as measured by the ADC are independent biological phenomena in newly diagnosed DLBCL. Further studies are warranted to assess the complementary roles of these different imaging biomarkers in the evaluation and follow-up of DLBCL.

**Keywords:** FDG-PET, diffusion-weighted MRI, standardized uptake value, apparent diffusion coefficient, diffuse large B-cell lymphoma

## Introduction

In 2013, an estimated number of 69,740 new cases will be diagnosed with non-Hodgkin lymphoma in the United States [1]. Diffuse large B-cell lymphoma (DLBCL) is the most common subtype, representing approximately one third of all non-Hodgkin lymphomas [2]. $^{18}$F-fluoro-2-deoxy-D-glucose positron emission tomography (FDG-PET) plays an important role in the evaluation of DLBCL [3, 4]. Aggressive lymphomas such as DLBCL have an increased glycolysis (mainly due to the overexpression of glucose membrane transporters and increased hexokinase activity), and this forms the basis for PET imaging with FDG [5]. Pretreatment FDG-PET is recommended in DLBCL, both for improved staging and in view of the evaluation of treatment response according to the revised Cheson criteria [6-8]. Interestingly, the degree of pre-

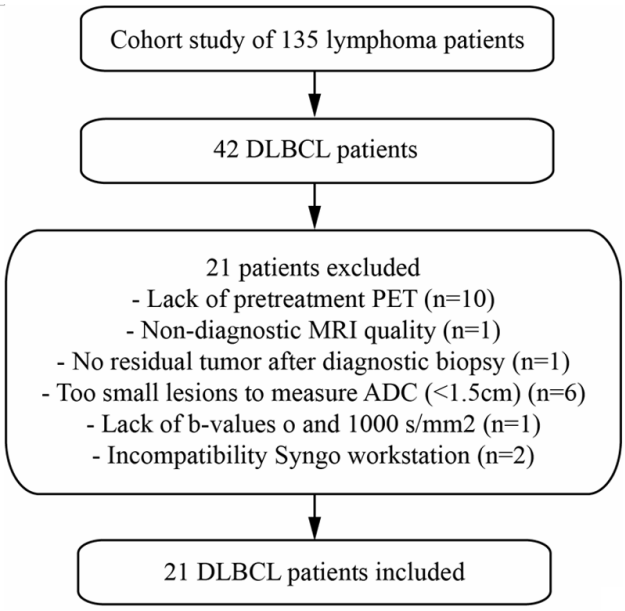


**Figure 1.** Flow diagram of included patients.

treatment volume-based FDG uptake in DLBCL has recently been reported to be a powerful predictor of outcome, surpassing the International Prognostic Index (IPI) score [9].

Meanwhile, diffusion-weighted magnetic resonance imaging (MRI) has been developed into a mature technique for staging lymphoma [10-13]. Diffusion-weighted MRI allows detection of microscopic changes in water mobility as a result of abnormalities of tissue structure at the cellular level, before gross anatomical changes become visible [14]. A recent study in Hodgkin lymphoma reported the pretreatment apparent diffusion coefficient (ADC; a quantitative measure of water diffusivity) to be predictive of site-specific interim response to chemotherapy [15].

Although both pretreatment FDG-PET and diffusion-weighted MRI are emerging as potentially useful prognostic biomarkers in DLBCL, their relationship has not been completely clarified yet. The limited previous studies show conflicting results. One study in 15 DLBCL patients reported no correlations between the pretreatment $ADC_{mean}$ and the $SUV_{max}$ or $SUV_{mean}$ [16], whereas another study in eight DLBCL patients reported a statistically significant inverse correlation between the pretreatment $SUV_{max}$ and $ADC_{mean}$ [17]. Thus, the relationship between these metrics has not been completely clarified yet.

The aim of this prospective study was therefore to determine the correlation between the FDG-PET standardized uptake value (SUV) and the diffusion-weighted MRI ADC in newly diagnosed DLBCL.

## Materials and methods

### *Patients*

Patients were recruited from a larger cohort of 135 patients with newly diagnosed lymphoma (various histopathological subtypes) who had been included in a prospective multicenter study in which the value of whole-body MRI, including diffusion-weighted MRI, was compared to computed tomography (CT) for staging lymphoma [18]. Institutional review board approval was obtained and all patients provided written informed consent. The parent(s) or guardian(s) of all patients under 18 years of age also provided written informed consent. Inclusion criteria for the present study were: patients aged 8 years or older with newly diagnosed histologically proven DLBCL and the availability of a (routine clinical) pretreatment FDG-PET that was randomly performed within 0-29 days of whole-body MRI. Exclusion criteria were: patients with other diagnoses than DLBCL, patients who had already received anticancer chemo- and/or immunotherapy, no residual tumor after diagnostic biopsy, non-diagnostic (diffusion-weighted) MRI quality, lack of b-values of 0 and 1000 s/mm$^2$ to create ADC maps, lack of pretreatment FDG-PET, incompatibility of FDG-PET data for Siemens Syngo workstation analysis, and lesions that were too small (i.e. diameter <1.5 cm) to obtain reliable ADC or SUV measurements.

### *FDG-PET*

FDG-PET imaging was performed by using either a Biograph 40 True Point Siemens Healthcare PET-CT system (Meander Medical Center Amersfoort) or a Gemini TOF Philips PET-CT system (Academic Medical Center Amsterdam). Patients who were scanned with the former system (n=15) ingested an oral CT contrast agent before FDG-PET scanning, whereas those patients who were scanned with the latter system (n=6) received an i.v. CT contrast agent before FDG-PET scanning. Patients fasted for at least six hours before intravenous

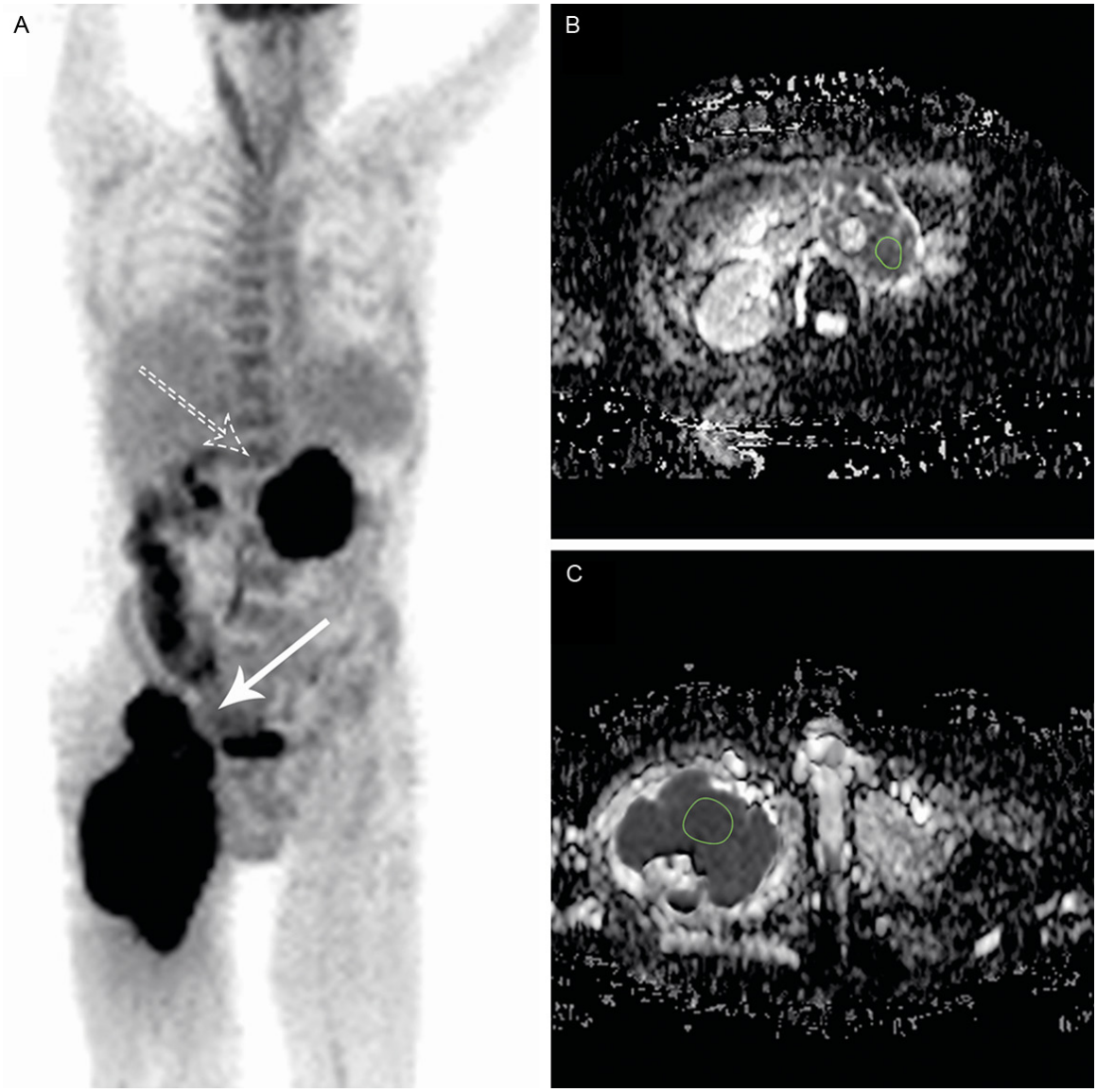


**Figure 2.** Coronal FDG-PET (A), axial ADC map at the para-aortic region (B), and axial ADC map at the inguinal region (C) in a 74-year-old man with newly diagnosed DLBCL. These images show lymphomatous involvement of confluent para-aortic lymph nodes (dashed arrow) and a large tumor mass in the right inguinal region extending into the right quadriceps femoris muscle (continuous arrow). The axial ADC maps show the single slice, transversal, manually drawn region of interest (ROI). $SUV_{max}$, $SUV_{mean}$, and $SUV_{peak}$ were measured in both the lesion with the visually highest FDG uptake and in the largest lesion. $ADC_{mean}$ was measured in the same lesions. SUVs were based on body weight and measurements were executed using the Siemens Syngo workstation (version VA11A), whereas ADC measurements were made using OsiriX DICOM Viewer (version 5.5.1). In this case, $SUV_{max}$ of the most FDG avid (para-aortic) and the largest (inguinal) lesion were 18.5 and 24.3, respectively. $ADC_{mean}$ of the most FDG avid and largest lesion was $0.61 \times 10^{-3}$ $mm^2/s$ and $0.43 \times 10^{-3}$ $mm^2/s$, respectively.

injection of 2.0-3.7 MBq/kg body weight FDG. Blood glucose levels were checked to be less than 11 mmol/L (i.e. less than 198 mg/dL) before injection. Images were acquired between 60-75 minutes after FDG injection. PET images were acquired with a 3D acquisition from the base of the skull to the mid-femur in five to seven bed positions, 2-3 minutes per bed position. Low-dose CT (Biograph 40 True Point) or full-dose CT (Gemini TOF) was used for attenuation correction of the PET images. PET images were reconstructed by OSEM iterative reconstruction (reconstruction matrix 128 × 128) and axial, sagittal, coronal and maximum inten-

**Table 1.** Baseline characteristics of included patients

| Patients | 21 |
|---|---|
| Sex | |
| Male | 14 |
| Female | 7 |
| Age | |
| Mean | 59 |
| Min-Max | 30-75 |
| Ann Arbor stage* | |
| Stage I | 3 |
| Stage II | 2 |
| Stage III | 3 |
| Stage IIIS | 2 |
| Stage IV | 11 |

Notes: *Ann Arbor stage based on FDG-PET and bone marrow biopsy results.

sity projections were created. The PET images were then co-registered (side-by-side display and software-based fusion) to low-dose (Biograph 40 True Point) or full-dose CT (Gemini TOF) images.

*Whole-body MRI*

Whole-body MRI, including diffusion-weighted MRI, was performed using either a Philips Achieva 1.5 T system or a Magnetom Avanto Siemens 1.5 T system. First, coronal multi-shot turbo spin-echo T1-weighted (repetition time [TR] of 537 ms, echo time [TE] of 18 ms) and T2-weighted short inversion time inversion recovery (STIR) (TR of 2444 ms, TE of 64 ms, inversion time [TI] of 165 ms) turbo spin-echo whole-body images were acquired using either the built-in body coil (Achieva) or the phased-array surface coils (Magnetom Avanto) for signal reception. Second, axial single-shot spin-echo echo-planar imaging diffusion-weighted images (TR of 6962 or 8612 ms, TE of 78 ms, TI of 180 ms, slice thickness/gap of 4/0 mm, field of view of 450 × 360 $mm^2$, matrix of 128 × 81, b-values 0 and 1000 $s/mm^2$) of the head/neck, chest, abdomen, and pelvis were acquired using phased-array surface coils for signal reception. Total actual data acquisition times were 12-15 minutes for T1-weighted images, 12-15 minutes for T2-weighted STIR images and 20-25 minutes for diffusion-weighted images with a total examination time of 45-55 minutes. ADC maps were created using b-values of 0 and 1000 $s/mm^2$.

*Image analysis*

All FDG-PET and magnetic resonance images were quantitatively assessed by one of the authors (AdJ), who was trained by two specialists in PET and diffusion-weighted MRI (both with >5 years of experience). Time interval between SUV and ADC measurements was at least 7 days, and the reviewer was blinded to ADCs when measuring SUVs (and vice versa). First, FDG-PET scans in each patient were reviewed to identify the malignant lesion with visually highest FDG uptake and the largest lesion. One single lesion could be identified as having both the visually highest FDG uptake and the largest size. In each patient, maximum SUV ($SUV_{max}$), mean SUV ($SUV_{mean}$) and peak SUV ($SUV_{peak}$, average SUV in 1 $cm^3$ volume sphere centered around the hottest pixel) were measured in both the lesion with the visually highest FDG uptake and in the largest lesion. Mean ADC ($ADC_{mean}$) was measured in the same lesions (**Figure 2**). SUVs were based on body weight and measurements were executed using the Siemens Syngo workstation (version VA11A), whereas ADC measurements were made using OsiriX DICOM Viewer (version 5.5.1). All measurements were based on a single slice (taking into account the partial volume effect), transversal, manually drawn region of interest (ROI) ranging from 113 $mm^2$ to 1871 $mm^2$ with a minimum pixel count of 20.

*Statistical analysis*

The Shapiro-Wilk test was used to check whether the SUV and ADC measurements were normally distributed, with a *W* statistic <0.90 considered to be statistically significant.

Subsequently, correlations between FDG-PET metrics ($SUV_{max}$, $SUV_{mean}$, $SUV_{peak}$) and $ADC_{mean}$ were assessed using Pearson's correlation coefficients, with *P*-values <0.05 considered to be statistically significant. All data were analyzed using the Statistical Package for the Social Sciences version 20.0 software (SPSS Inc., IL, USA).

## Results

A total of 42 patients with newly diagnosed DLBCL were potentially eligible for inclusion. Ten of these patients were excluded because of the lack of pretreatment FDG-PET. One patient

**Table 2.** FDG-PET metrics and $ADC_{mean}$ ($10^{-3}$ $mm^2/s$) of included patients (mean±SD)

| | $SUV_{max}$ | $SUV_{mean}$ | $SUV_{peak}$ | $ADC_{mean}$ |
|---|---|---|---|---|
| Most FDG avid lesion | 23.8±8.2 | 16.9±6.6 | 19.5±7.3 | 0.7±0.1 |
| Largest lesion | 22.6±7.9 | 16.2±6.4 | 18.6±6.8 | 0.71±0.15 |

was excluded because of non-diagnostic (diffusion-weighted) MRI quality, one patient was excluded because of tumor invisibility after diagnostic biopsy, six patients were excluded because lesions were too small (i.e. diameter <1.5 cm) to obtain reliable ADC measurements, and one patient was excluded because of the lack of b-values of both 0 and 1000 s/$mm^2$ to allow the creation of ADC maps. Finally, two patients were excluded because of incompatibility of FDG-PET data for Syngo workstation analysis. Thus, 21 patients with newly diagnosed DLBCL (14 men and 7 women, mean age: 59 years, range 30-75 years, scanned between August 2008 and November 2011) were finally included in this study (**Figure 1**). Patient characteristics are displayed in **Table 1**.

Shapiro-Wilk tests confirmed that the $SUV_{max}$, $SUV_{mean}$, $SUV_{peak}$, and $ADC_{mean}$ (both in the visually most FDG avid lesion and in the largest lesion) were normally distributed (W-statistics ≥0.92 for all metrics). Mean±standard deviation (SD) of $SUV_{max}$, $SUV_{mean}$, $SUV_{peak}$, and $ADC_{mean}$ ($10^{-3}$ $mm^2/s$) in the visually most FDG avid lesion were 23.8±8.2, 16.9±6.6, 19.5±7.3 and 0.7±0.1 respectively (**Table 2**). Mean±SD of $SUV_{max}$, $SUV_{mean}$, $SUV_{peak}$, and $ADC_{mean}$ ($10^{-3}$ $mm^2/s$) in the largest lesion were 22.6±7.9, 16.2±6.4, 18.6±6.8 and 0.71±0.15 respectively (**Table 2**). In the lesions with visually highest FDG uptake, no significant correlations were found between the $SUV_{max}$, $SUV_{mean}$, $SUV_{peak}$ and the $ADC_{mean}$ ($P$=0.498, $P$=0.609 and $P$=0.595, respectively) (**Figure 3**). In the largest lesions, there were no significant correlations either between the $SUV_{max}$, $SUV_{mean}$, $SUV_{peak}$ and the $ADC_{mean}$ ($P$=0.992, $P$=0.843 and $P$=0.894, respectively) (**Figure 3**). Besides the correlation between FDG-PET and DWI-MRI we also evaluated the correlation between different FDG-PET biomarkers. In both the FDG most avid lesions as in the largest lesions there was a significant correlation between the $SUV_{max}$ and $SUV_{mean}$ ($P$=0.991 and $P$=0.953 respectively) (**Figure 4**).

## Discussion

In this study, no correlations were found between the FDG-PET SUV and the diffusion-weighted MRI ADC in newly diagnosed DLBCL. The biological meaning of these findings, however, is still unclear. Although the FDG-PET SUV is generally thought to reflect tumor cellular proliferation [19], the biophysical basis of the ADC is less clear. Classically, the low ADCs found in most tumors have been attributed to their increased cellular density; however, this remains a point of contention because diffusivity can also be influenced by extracellular fibrosis, the shape and size of the intercellular spaces, and by other microscopic tissue/tumor organizational characteristics [14]. Interestingly, a recent study found no correlation between the ADC and cellularity of the tumor in DLBCL [20]. Thus, more histological and immunohistochemical studies are required to clarify the biophysical correlate(s) of the ADC in relationship to FDG-PET metrics. On a clinical level, pretreatment quantitative FDG-PET is emerging as a powerful predictor of outcome in DLBCL [9]. Although a similar role for pretreatment diffusion-weighted MRI still has to be established in DLBCL, a recent study in Hodgkin lymphoma reported the pretreatment ADC to be predictive of site-specific interim response to chemotherapy [15]. The lack of a relationship between pretreatment FDG-PET and diffusion-weighted MRI metrics might indicate a complementary role of these two imaging modalities for pretreatment risk stratification and early response assessment in DLBCL. Further studies are required to investigate these hypotheses.

Similar to our findings, a previous study by Wu et al. found no correlations between the pretreatment $ADC_{mean}$ and the $SUV_{max}$ or $SUV_{mean}$ in 15 DLBCL patients [16]. However, another study by the same research group did find a significant relationship between pretreatment FDG-PET and diffusion-weighted MRI metrics [17]. In eight patients with DLBCL, $ADC_{mean}$ correlated inversely with the $SUV_{max}$ ($r$=-0.74, $P$<0.05 when measuring in the center of pathological lymph nodes and $r$=-0.71, $P$<0.05 when measuring in the periphery of pathological lymph nodes). The low number of patients and the inclusion of both primary and relapsed DLBCL may have caused these conflicting

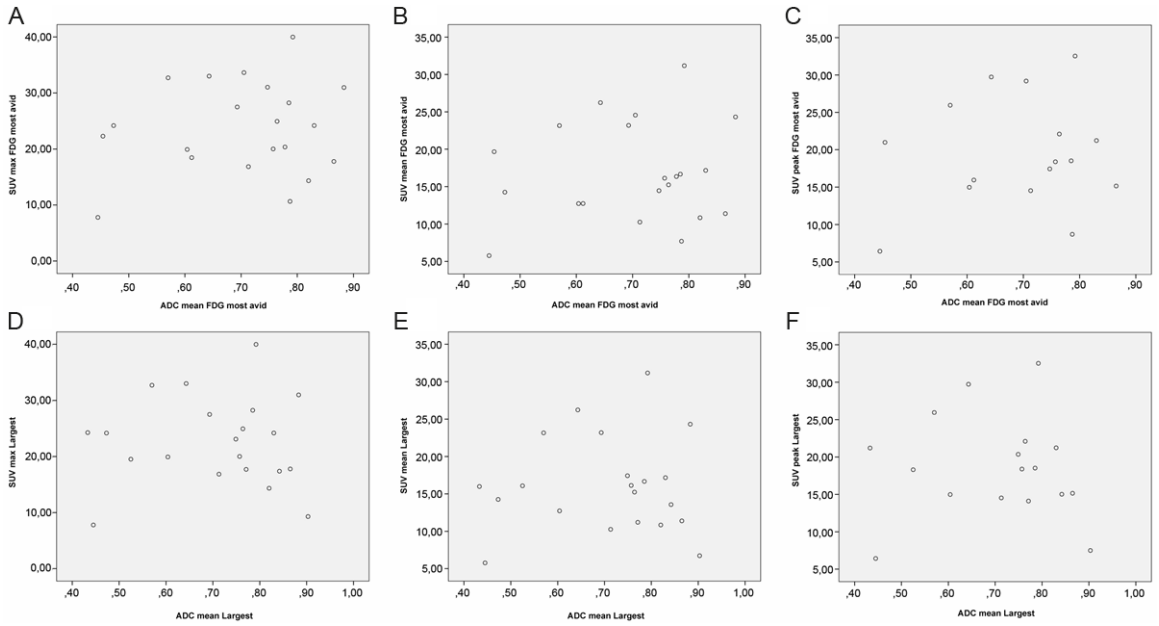


**Figure 3.** Scatter plots of FDG-PET metrics ($SUV_{max}$ (A, D), $SUV_{mean}$, (B, E) and $SUV_{peak}$ (C, F) versus $ADC_{mean}$ (in $10^{-3}$ $mm^2/s$) for the most FDG avid lesions (A-C) and largest lesions (D-F). No significant correlations were found ($P \geq 0.498$ for all comparisons).

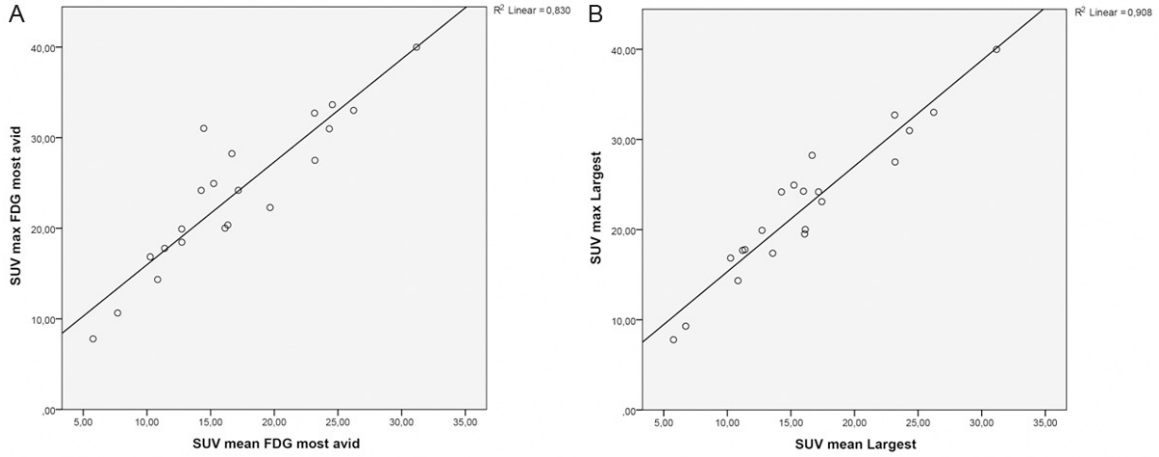


**Figure 4.** Scatter plots of FDG-PET metrics $SUV_{max}$ and $SUV_{mean}$ for the most FDG avid lesions (A) and largest lesions (B) ($P$=0.991 and $P$=0.953 respectively).

results. However, the present study indicates that such a relationship does not exist.

The present study had several limitations. First, the study population was relatively small. Nevertheless, it consisted of a prospectively recruited, homogeneous group of newly diagnosed DLBCL patients. Second, different PET-CT and MRI systems were used, which may have influenced SUV and ADC measurements. It is imperative for future studies to apply a standardized, minimum set of requirements for PET-CT and MRI scanning and continuing quality control. Of interest, although the recently introduced EARL FDG-PET/CT accreditation programme serves this purpose for quantitative PET-CT scanning [5], such an accreditation programme still has to be developed for ADC measurements. Third, only one reader performed all measurements, but blinding for both measurements was assured by introducing a time interval of at least 7 days between the

SUV and ADC measurements. Interrater agreement analysis of SUV and ADC measurements, however, was not part of this study and needs further investigation. Fourth, SUV and ADC measurements could not be correlated to histological and immunohistochemical results because diagnostic lymph node excision had been performed before the FDG-PET and MRI examinations. In conclusion, the results of this study indicate that the glycolytic rate as measured by FDG-PET and changes in water compartmentalization and water diffusion as measured by the ADC are independent biological phenomena in newly diagnosed DLBCL. Further studies are warranted to assess the complementary roles of these different imaging biomarkers in the evaluation and follow-up of DLBCL.

## Acknowledgements

This project was financially supported by the Dutch Organization for Health Research and Development (ZonMw) Program for Health Care Efficiency Research (grant number 80-82310-98-08012) and by an Alpe d'HuZes/Dutch Cancer Society Bas Mulder Award for T.C.K. (grant number 5409). Data collection, data analysis and interpretation of data, writing of the paper, and decision to submit were left to the authors' discretion and were not influenced by ZonMw or Alpe d'HuZes/Dutch Cancer Society.

## Disclosure of conflict of interest

None (all authors).

**Address correspondence to:** Antoinette de Jong, Department of Radiology and Nuclear Medicine, University Medical Center, Utrecht, The Netherlands. E-mail: jong.de.an@gmail.com

## References

[1] Siegel R, Naishadham D, Jemal A. Cancer Statistics, 2013. CA Cancer J Clin 2013; 63: 11-30.

[2] Flowers CR, Sinha R, Vose JM. Improving Outcomes for Patients with Diffuse Large B-Cell Lymphoma. CA Cancer J Clin 2010; 60: 393-408.

[3] Delbeke D, Stroobants S, de Kerviler E, Gisselbrecht C, Meignan M, Conti PS. Expert Opinions on Positron Emission Tomography and Computed Tomography Imaging in Lymphoma. Oncologist 2009; 14: 30-40.

[4] Miyazaki Y, Nawa Y, Miyagawa M, Kohashi S, Nakase K, Yasukawa M, Hara M. Maximum standard uptake value of 18F-fluorodeoxyglucose positron emission tomography is a prognostic factor for progression-free survival of newly diagnosed patients with diffuse large B cell lymphoma. Ann Hematol 2013; 92: 239-44.

[5] Boellaard R, O'Doherty MJ, Weber WA, Mottaghy FM, Lonsdale MN, Stroobants SG, Oyen WJG, Kotzerke J, Hoekstra OS, Pruim J, Marsden PK, Tatsch K, Hoekstra CJ, Visser EP, Arends B, Verzijlbergen FJ, Zijlstra JM, Comans EFI, Lammertsma AA, Paans AM, Willemsen AT, Beyer T, Bockisch A, Schaefer-Prokop C, Delbeke D, Baum RP, Chiti A, Krause BJ. FDG PET and PET/CT: EANM procedure guidelines for tumour PET imaging: version 1.0. Eur J Nucl Med Mol Imaging 2010; 37: 181-200.

[6] Tilly H, Vitolo U, Walewski J, Gomes da Silva M, Shpilberg O, André M, Pfreundschuh M, Dreyling M. Diffuse large B-cell lymphoma (DLBCL): ESMO Clinical Practice Guidelines for diagnosis, treatment and follow-up. Ann Oncol 2012; 23: 78-82.

[7] Juweid ME, Stroobants S, Hoekstra OS, Mottaghy FM, Dietlein M, Guermazi M, Wiseman GA, Kostakoglu L, Scheidhauer K, Buck A, Naumann R, Spaepen K, Hicks RJ, Weber WA, Reske SN, Schwaiger M, Schwartz LH, Zijlstra JM, Siegel BA, Cheson BD. Use of Positron Emission Tomography for Response Assessment of Lymphoma: Consensus of the Imaging Subcommittee of International Harmonization Project in Lymphoma. J Clin Oncol 2007; 25: 571-578.

[8] Quarles van Ufford H, Hoekstra O, de Haas M, Fijnheer R, Wittebol S, Tieks B, Kramer M, de Klerk J. On the Added Value of Baseline FDG-PET in Malignant Lymphoma. Mol Imaging Biol 2010; 12: 225-232.

[9] Kim TM, Paeng JC, Chun IK, Keam B, Jeon YK, Lee S, Kim DW, Lee DS, Kim CW, Chung JK, Kim IH, Heo DS. Total Lesion Glycolysis in Positron Emission Tomography Is a Better Predictor of Outcome Than the International Prognostic Index for Patients With Diffuse Large B Cell Lymphoma. Cancer 2013; 119: 1195-1202.

[10] Kwee TC, Quarles van Ufford HME, Beek FJ, Takahara T, Uiterwaal CS, Bierings MB. Whole-body MRI, Including Diffusion-Weighted Imaging, for the Initial Staging of Malignant Lymphoma: Comparison to Computed Tomography. Invest Radiol 2009; 44: 683-690.

[11] Punwani S, Taylor SA, Bainbridge A, Prakash V, Bandula S, De Vita E, Olsen OE, Hain SF, Stevens N, Daw S, Shankar A, Bomanji JB, Humphries PD. Pediatric and Adolescent Lymphoma: Comparison of Whole-Body STIR Half-

Fourier RARE MR Imaging with an Enhanced PET/CT Reference for Initial Staging. Radiology 2010; 255: 182-190.

[12] Lin C, Luciani A, Itti E, El-Gnaoui T, Vignaud A, Beaussart P, Lin SJ, Belhadj K, Brugières P, Evangelista E, Haioun C, Meignan M, Rahmouni A. Whole-body diffusion-weighted magnetic resonance imaging with apparent diffusion coefficient mapping for staging patients with diffuse large B-cell lymphoma. Eur Radiol 2010; 20: 2027-2038.

[13] Velasco S, Burg S, Delwail V, Guilhot J, Perdrisot R, Guilhot FR, Tasu JP. Comparison of PET-CT and magnetic resonance diffusion weighted imaging with body suppression (DWIBS) for initial staging of malignant lymphomas. Eur J Radiol 2013; 82: 2011-2017.

[14] Padhani AR, Liu G, Koh DM, Chenevert TL, Thoeny HC, Takahara T, Dzik-Jurasz A, Ross BD, van Cauteren M, Collins D, Hammoud DA, Rustin GJS, Taouli B, Choyke PL. Diffusion-Weighted Magnetic Resonance Imaging as a Cancer Biomarker: Consensus and Recommendations. Neoplasia 2009; 11: 102-125.

[15] Punwani S, Taylor SA, Saad ZZ, Bainbridge A, Groves A, Daw S, Shankar A, Halligan S, Humphries PD. Diffusion-weighted MRI of lymphoma: prognostic utility and implications for PET/MRI? E Eur J Nucl Med Mol Imaging 2013; 40: 373-385.

[16] Wu X, Korkola P, Pertovaara H, Eskola H, Järvenpää R, Kellokumpu-Lehtinen PL. No correlation between glucose metabolism and apparent diffusion coefficient in diffuse large B-cell lymphoma: A PET/CT and DW-MRI study. Eur J Radiol 2011; 79: e117-e121.

[17] Wu X, Kellokumpu-Lehtinen PL, Pertovaara H, Korkola P, Soimakallio S, Eskola H, Dastidar P. Diffusion-weighted MRI in early chemotherapy response evaluation of patients with diffuse large B-cell lymphoma – a pilot study: comparison with 2-deoxy-2-fluoro-D-glucose-positron emission tomography/computed tomography. NMR Biomed 2011; 24: 1181-1190.

[18] Kwee TC, Vermoolen MA, Akkerman EA, Kersten MJ, Fijnheer R, Ludwig I, Beek FJA, Van Leeuwen MS, Bierings MB, Bruin MCA, Zsíros J, Quarles van Ufford HME, De Klerk JMH, Adam J, Stoker J, Uiterwaal CS, Nievelstein RA. Whole-body MRI, including diffusion-weighted imaging, for staging lymphoma: comparison with CT in a prospective multicenter study. J Magn Reson Imaging 2013; [Epub ahead of print].

[19] Wu X, Pertovaara H, Korkola P, Vornanen M, Eskola H, Kellokumpu-Lehtinen PL. Glucose metabolism correlated with cellular proliferation in diffuse large B-cell lymphoma. Leuk Lymphoma 2012; 53: 400-405.

[20] Wu X, Pertovaara H, Dastidar P, Vornanen M, Paavolainen L, Marjomäki V, Järvenpää R, Eskola H, Kellokumpu-Lehtinen PL. ADC measurements in diffuse large B-cell lymphoma and follicular lymphoma: a DWI and cellularity study. Eur J Radiol 2013; 82: e158-164.